RESPONSES OF BANGKOK SUBSOIL DUE TO EARTHQUAKES

Satoshi MORIO[1], Yoshinori KATO[2], Akira KITAZUMI[3]
Supot TEACHAVORASINSKUN[4] and Punya CHARUSIRI[5]

ABSTRACT: Bangkok subsoil is believed to amplify long period components of the far field earthquakes occurred from a source with a few hundred kilometers away from the city. The reason of this amplification characteristic is mostly due to the nature of the Bangkok subsoil profiles. In the present study, the maximum credible earthquake induced by the Three Pagoda fault which is one of the closest active fault to Bangkok Metropolitan was evaluated. Then the waveform of the generated strong ground motion was formulated and the ground motion at Bangkok was computed based on the linear equivalent model. It was found that the predominant period of about 0.7 sec was obtained from the surface ground motion.

Key words: Bangkok soil layers, Active fault, Dynamic response analysis, Empirical Green's function method, Osaki's spectrum

1. Introduction

Earthquakes of M6.1 induced from the active fault nearby the borderline between Laos and Myanmar in May 16, 2007 event resulted in damages of several civil structures in Chiang-Mai (about 260 km from the epicenter). At the same time, most highlight buildings in Bangkok which located 750 km away from the center of quakes also clearly underwent low frequency shaking. According to the report of the Southeast Asia Association of Seismology and Earthquake Engineering[1)], far field earthquakes can easily induce a long period motion in the Bangkok subsoil. This is due to the characteristic of soft ground underlain Bangkok.

In 1985, the M8.1 Mexico earthquake has destroyed the Mexico City which is located 350 km from the epicenter. About 6,000 people were killed in that event. The Mexico City has been underlain by a very thick soft clay deposit. This thick soft clay, together with the basin nature of its rock base, greatly amplified that distant shake. The top of Bangkok subsoils are generally covered with the very soft clay with the thickness of 15 – 20 m. Under this soft deposit are layers of stiff to hard clays and dense sands to base rock.

In the present study, the influence of the closest active fault (the Three Pagoda fault) on the ground shaking of Bangkok will be evaluated. The procedures adopted in this study are;

(1) Waveform generation based on the Empirical Green's function method

(2) Waveform generation based on the Osaki's spectrum

After obtaining the strong ground motion, the ground response at Bangkok metropolitan will be computed based on the linear equivalent analysis of horizontal ground. This surface ground motion can then be used as the input for structural response analysis.

2. Recorded earthquakes in Southeast Asian region and active faults nearby Thailand

The recorded earthquakes in Southeast Asian region during 1446 – 1999 are summarized in **Fig.1**[2)]. The subduction zone between the Indo-Australian plate and the Eurasia plate is also depicted in the figure for reference, as well as the epicenter of December 26, 2004 M9.0 earthquake.

It has been well recognized that the denser Indo-Australian plate is subducted into the lighter Eurasia plate. The Eurasia plate is then carrying great collision pressures from the Indo-Australian plate. As a consequence, considerable number of active faults has been found in the east side of the plate boundary. However, those faults have been fortunately bounded by the Red-River fault (north of Vietnam). The active faults are therefore concentrated in Myanmar and its Northern boundaries between Thailand, Laos and China as shown in the figure.

1 Professor, Department of Civil Engineering, Maizuru National College of Technology
2 Lecturer, Department of Civil Engineering, Maizuru National College of Technology
3 JICA SV, Department of Mineral Resources, Thailand
4 Assistant Professor, Department of Civil Engineering, Chulalongkorn University
5 Assistant Professor, Department of Geology, Chulalongkorn University

Table 1 Historical earthquakes in Thailand

Date	Location where the event was observed	Intensity (MM Scale) and/or Magnitude	Remarks
624 BC.	Chian Saen	6	
623 BC.	Chian Saen	6	
594 BC.	Chian Saen	6	
589 BC.	Chian Saen	6	
460	Chian Saen	12	The whole town submerged and became a big lake; The king and all of his subjects died exept one old widow.
534	Chian Saen	8	Four pagodas were toppled.
1362	Sukhothai	6	
1366	Sukhothai	5	
1482	Chiang Mai	6	
1505	Ayuthaya	6	
1527	Ayuthaya	?	
1545	Chiang Mai	7	Great pagoda(H=86m) was toppled and only 60 odd metres were left standing
1546	Ayuthaya	?	
1568	Rangoon	8	The Rangon Pagoda was toppled down to the middle part
1584	Ayuthaya	6	
1588	Ayuthaya	6	
1629	Rangoon	7	
1661	Rangoon	7	
1664	Rangoon	9	
1685	Ayuthaya	5	
1689	Ayuthaya	6	
1715	Chiang Saen	7	The temples and pagoda in four districts were destroyed
1715	Chieng Mai	6	
1739	Pegu	9	
1757	Pegu	9	
19/Dec/1768	Bangkok	6	
02/Apl/1769	Bangkok	5	
1774	Chiang Mai	5	
16/Jul/1799	Bangkok	5	
07/Nov/1799	Bangkok	5	
24/Feb/1832	Bangkok	5	
22/Oct/1833	Bangkok	5	
24/Nov/1833	Bangkok	6	
26/Mar/1835	Bangkok	6	
26/Aug/1835	Bangkok	5	
16/Mar/1839	Bangkok	?	
14/Oct/1841	Bangkok	5	
16/Feb/1860	Bangkok	5	
03/Mar/1874	Bangkok	5	
06/Feb/1886	Bangkok	6	
22/Nov/1886	Bangkok	6	
30/Nov/1887	Bangkok	5	
21/Mar/1959	Kanchanaburi	?	Ground Crack was observed at Klondo subdistrict of the town of Kanchanaburi to be about 300m long and 1-2m wide and fountains of water ejected.
17/Feb/1975	17.6N,97.9E	M5.9	Slight damage and injury in Bangkok. Slight damege and Crack on Phra That Phanom Pagoda and was inclined.
25/may/1978	19.3N,99.1E	M4.8	Slight damage in Phrao
01/Sep/1978	20.44N,100.6E	M4.9	
30/Sep/1978	Ranong Fault	M5.6	
22/Apl/1983	14.95N,99.07E	M5.8	Slight damage in Bangkok, Nakon Pathom, Kanchanabuli. Land Slide and Ground Crack were found in Kanchanabuli.
11/Sep/1994	Chiang Rai	M5.1	Medium damage on Hospital which is 20-25Km from Epicenter.
9/Dec/1995	Phrae	M5.1	Slight damage on School and pagoda.
21/Dec/1995	Chiang Mai	M5.2	Slight damage on School and pagoda.

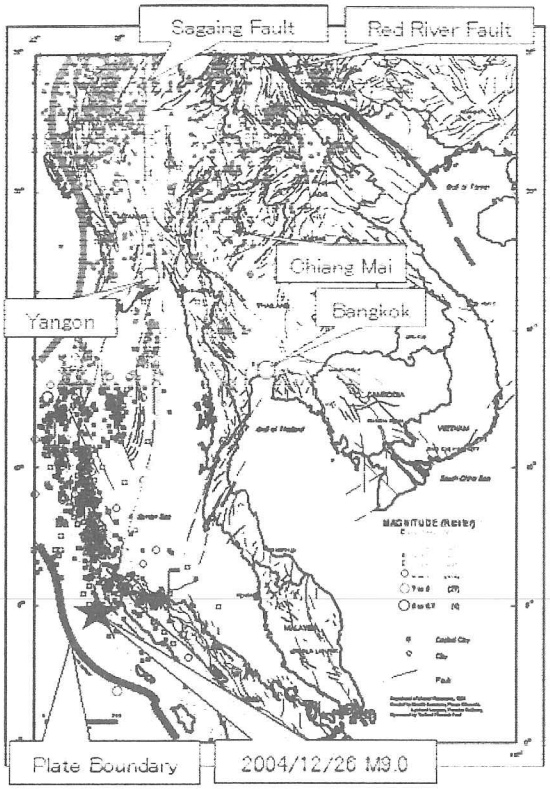

Fig.1 Faults and earthquake epicenters in Thailand and South East Asia

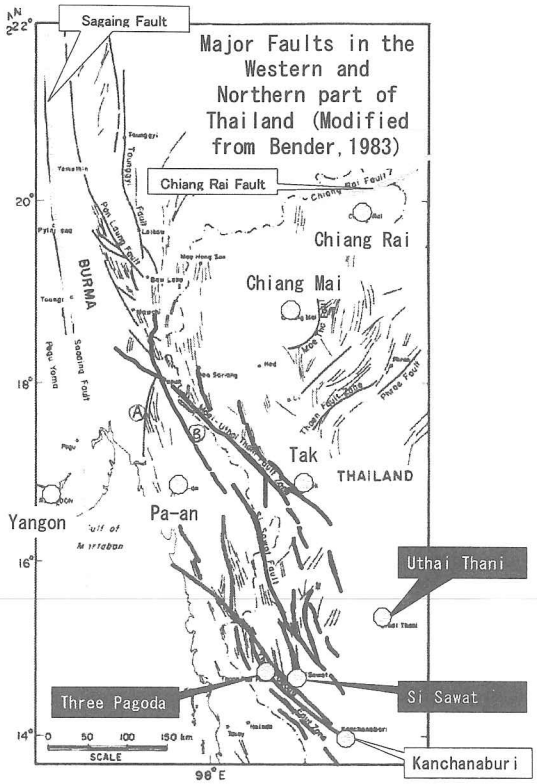

Fig.2 Major faults in the Western and Northern part of Thailand

The active faults found in the western and northern parts of Thailand are shown in **Fig.2**[3]. There are currently recognized that the Moei fault, Si Sawat fault, Three pagoda fault and Chiang Rai fault are still active. **Figs. 1** and **2** show the location of the Sagaing fault which has been the causes of several events of large earthquakes in the past. This right-lateral fault is one of the known active faults in the area. Those previous mentioned three active faults found in Thailand are segments of this Sagaing fault.

In the past, it had been believed that Thailand was not susceptible to earthquake damages. However, as shown in **Table 1**, there were at least three earthquakes of magnitude 6.0 being recorded by SEASEE and TMD (Thailand Meteorological Department). Based on the information shown in **Table 1**, there was a very large earthquake occurring in the year 460 (AD) in Chiang Rai province. The earthquake was believed to propagate from the Chiang Rai Fault. With this shaking, the top part of the famous JADYLUANG pagoda had been torn down. It should be noted that most records shown in the table are adapted from SEASEE. Thailand has been officially establishing the network of seismograph since 1960. Since then, considerable numbers of earthquakes of magnitude 5 has been recorded. With this network, TMD is able to locate the epicenter of the earthquakes at which the historical events could not tell. Furthermore, the standard magnitude scale has been used since then.

In the present study, the potential of the Three Pagoda faults to generate strong ground shaking shall be estimated. It is believed that the Si Sawat fault (main sector of Three Pagoda fault) extends its alignment through Bangkok and Samut Sakhorn. The Three Pagoda fault has been continuously explored in these few years. It is very important to prove whether the fault could extend closer to Bangkok Metropolitan or not.

3. Analytical methods

To estimate the strong motion producing from an active fault can be done using the following two procedures.

3.1 Empirical Green's Function method

The procedure has been proposed by Hertzel,S.H.[4] and Irikura, K.[5]. The flowchart showing its procedure is summarized in **Fig.3**. In this method, several parameters indicate the earthquake size and source characteristics, together with the actual record of small to medium size earthquakes generated from that source, being designated by the Green's function. Since the usage of actual small earthquakes from the

targeted source, the computed strong ground motion was found to be close to realistic.

Unfortunately, there has no actual record of small earthquake from the targeted fault. The ω^{-2} model proposed by Boore, D.M.[6] was then adopted to generate the time history motion of the small to medium size earthquake. The ω^{-2} model adopts the white noise filter to generate waveform from the frequency spectrum of the motion. This method is also called the stochastic model. It should be noted that proposed local site effect must be further treated using the finite element method.

Due to the non-uniformity of the mass rock density inside the active fault, there is a parameter called asperity must be considered. The short period motions are usually generated from the location where rock mass density is large. Due to the lack of information, the asperity was not considered in the analysis of the present study.

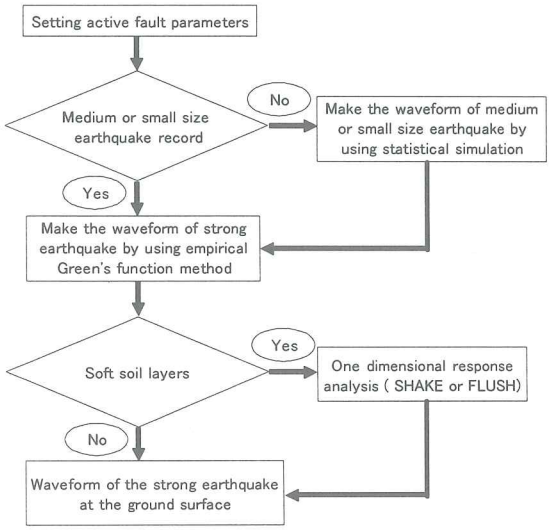

Fig.3 Analytical flow

3.2 Estimation of waveform from Osaki's spectrum

The Osaki's spectrum is the velocity response spectrum derived from actual records obtained on the rock outcrop (shear wave velocity of 1.3±0.4 km/s) with damping ratio of 5%. The spectrum is then related as a function of earthquake magnitude and distance from the source. Based on this targeted spectrum, the fitting procedure[7] is then adopted to produce the strong ground motion at proposed site.

Table 2 Fault parameters (small size earthquake)

Data	Unit	Explanation
5	km	Length
4	km	Width
N135E	degree	Strike
90	degree	Dip
180	degree	Lake (right-lateral)
0.63		Radiation coefficient
2.0		Influence of ground surface
9.68	Hz	Max frequency of height cut filter
0.71		PRTITN (Energy distribution of two horizontal components)
2.7	g/cm^3	Density
3.5	km/sec	Shear wave velocity
50.0	bar	Stress drop
50.0	km	Focal Distance
9.636E+23	dyne-cm	Seismic Moment
5.25		Moment Magnitude

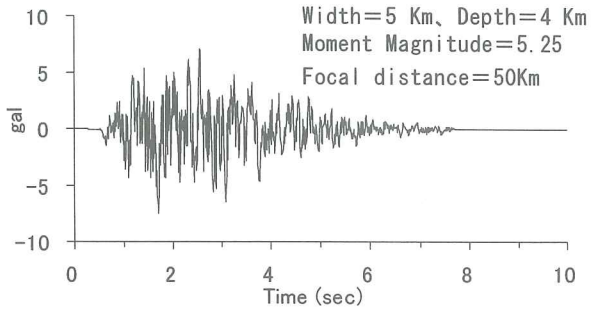

Fig.4 Small size earthquake waveform

4. Strong ground motion at Bangkok base rock

4.1 Strong ground motion using the empirical Green's function

Tables 2 and **3** summarize the parameters and formulation adopted for prediction of waveform of the small earthquake of moment magnitude of 5.25. The active fault is assumed to be right-lateral with 5 km long and 4 km width.

The computed time history motion (acceleration time history) of the small earthquake based on the stochastic model is shown in **Fig.4**. The comparison of

Table 3 How to decide fault parameters

S (km^2)	Area of fault	L×W L : Length in strike direction W : Length in dip direction	
Mo (dyne-cm)	Moment magnitude	$S=2.05\times10-15\cdot Mo^{2/3}$	Somerville[8]
M	Magnitude	$\log Mo=1.164M+17.874$	
τ (sec)	Rise time	$\tau=1.72\times10^{-9}\cdot Mo^{1/3}$	Somerville[8]
fmax (Hz)	Max frequency of height cut filter	$fmax=7.31\times10^{3}\times Mo^{-0.12}$	Faccioli[9]
TD	Duration time	$TD=10^{(0.31M-0.77)}$	
Qs	Q value	$Qs=142.9\times f^{0.85}$	
fc	Corner frequency	$fc=4.9\times106\times\beta\times(\Delta\sigma/Mo)^{1/3}$	Brune[10]

the acceleration Fourier spectrum of the targeted spectrum (omega spectrum) and the obtained waveform the white noise filter is also shown in **Fig.5**.

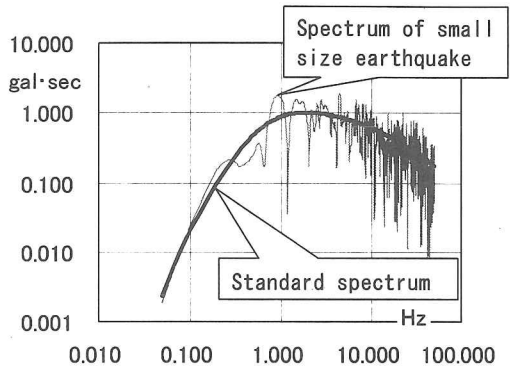

Fig.5 Fourier spectrum

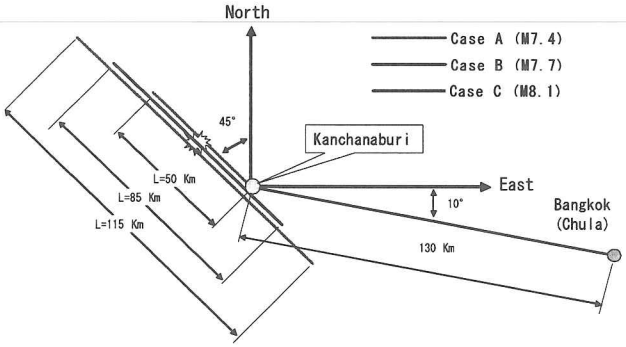

Fig.6 Configuration of the Three Pagoda Fault

Adopting the small earthquake ground motion shown in **Fig.4**, the strong ground motion at the rock base of Bangkok can be predicted using the empirical Green's function. Since the Three Pagoda fault parameters (fault characteristics) is not very clear, three cases of the fault characteristics are then used (Case A, B and C as shown in **Fig.6**). The faults length and width of 50 km and 20 km (M7.4) for case A, 85 km and 20 km (M7.7) for case B and 115 km and 30 km (M8.1) for case C were selected. These are summarized in **Table 4**. The number of superimposed when compared to the moment magnitude is 7x7 for case A, 9x9 for Case B and 13x13 for Case C. It is assumed that the targeted fault inclined by 90°and being right-lateral. In the present study, the rupture is always propagated from the central bottom of the fault. Once rupture starts, it is assumed the whole length of the segment collapses. Since the actual length of the Three Pagoda fault is about 80 km which is close to the condition adopted for Case B, the result from Case B should represent the actual strong ground motion. However, due to lacks of various important information, for examples, the recorded ground motion, fault and rock characteristics, Case A and Case C have been analyzed in order to carry the parametric study. It is therefore suggested that more information related to the fault must be gathered so that refine analysis, including the influence of asperity, should be done in the near future.

Table 4 Fault parameters (the Three Pagoda Fault)

Data	Unit	Explanation
N135E	degree	Strike
90	degree	Dip
180	degree	Rake rake=180 : right-lateral, rake= 0 : left-lateral, rake=-90 : normal fault, rake=90 : reverse fault
30	km	Focal Depth
115	km	Length of fault in strike direction
30	km	Length of fault in dip direction
2.231	sec	Rise time (fault slipping time)
13,13,13		Dividing number in strike, dip and time direction
7,13		Failure starting point in strike and dip direction
3.5	km/sec	Shear wave velocity
2.7	km/sec	Failure propagation velocity
2		Failure propagation style (1 : parallel propagation, 2 : radial propagation)
0		Correction of radiation pattern (0 : No correction, 1 : Correction, 2 : Correction of sign)
151	km	Epicentral distance
105	degree	Azimuth (Angle of vector connecting epicenter to obserbation point with North direction)
NS		Compornent of earthquake wave
2		Time integral function (1 : boxcar function, 2 : delta+boxcar function, 3 : delta+e function)
1.3		Stress drop ratio ($\Delta\sigma_B/\Delta\sigma_S$)

Fig.7 summarizes the acceleration time history of the strong motion computed using the above mentioned empirical Green's function method. The results depicted are those representing analytical Case A, Case B and Case C, respectively. The velocity spectrum with damping ratio of 5% of those strong motion obtained from all three cases are shown in **Fig.8**. For comparison reason, the velocity spectrum of the small earthquakes obtained using the stochastic method is also shown in the figure. **Table 5** summarizes the maximum acceleration obtained from the strong motions. The maximum acceleration and velocity generally increase with the increase in magnitude of earthquake. It can be seen from the time history that duration of shaking increases with

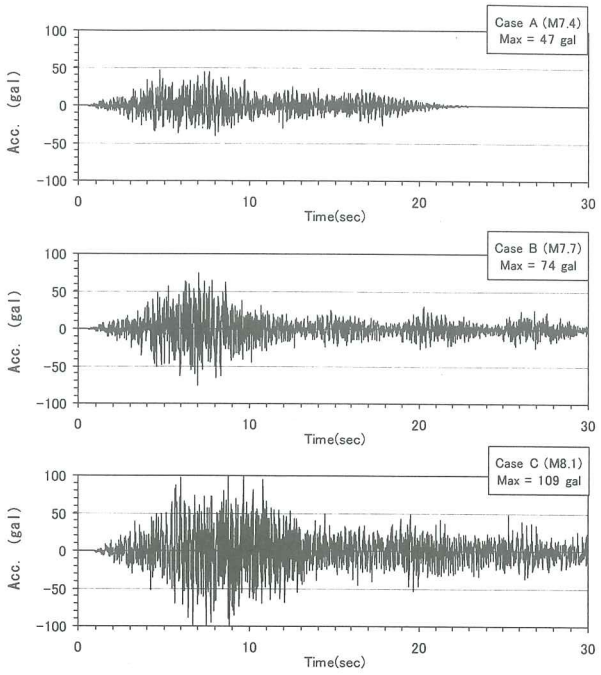

Fig.7 Acceleration time history

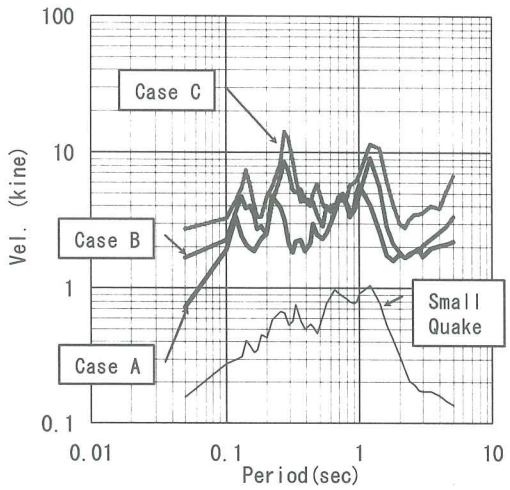

Fig.8 Velocity response spectrum

Table 5 Maximum response

Case	Acc.(gal)	Vel.(kine)
A (M7.4)	47.0	2.94
B (M7.7)	74.1	6.10
C (M8.1)	108.8	8.60

increasing in earthquake magnitude. Furthermore, the predominant period shifts towards the longer period when magnitude of earthquakes increases. Namely, the predominant periods of 0.14, 0.27 and 1.2 sec are obtained for Case A, B and C, respectively.

4.2 Influence of Directivility

As previously mentioned, the staring point of rupture for Case A, B and C is assumed to be at the center bottom of the fault. In order to investigate the influence of directivility, the rupture starting point of Case C is moved to the bottom north of fault (Case C1) and to the bottom south of the fault (Case C2) as schematically shown in **Fig.9**. It can be seen that for Case C1, the rupture propagates towards Bangkok, while for Case C2, the rupture of the fault propagates away from Bangkok.

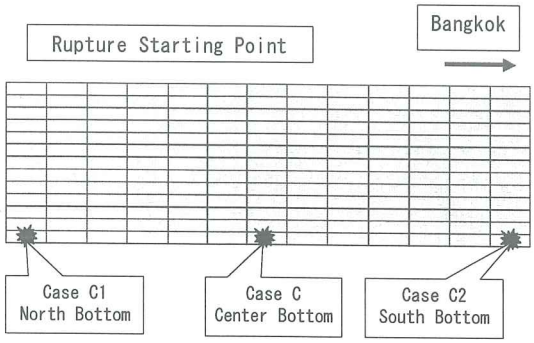

Fig.9 Rapture starting point

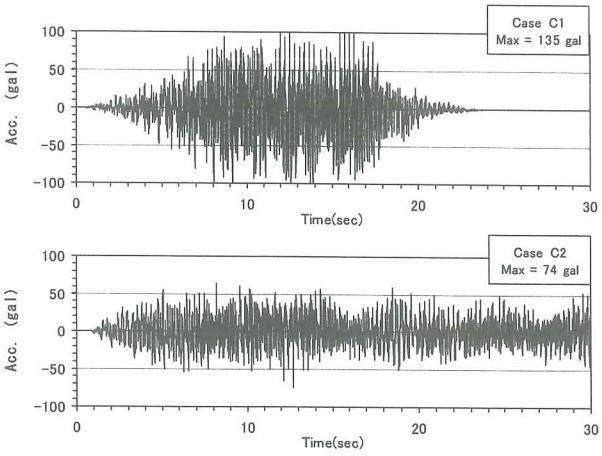

Fig.10 Acceleration time history

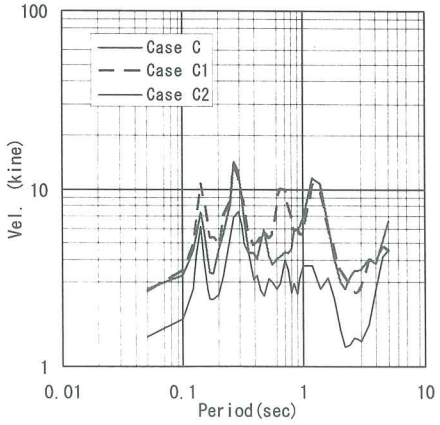

Fig.11 Velocity response spectrum

The acceleration time histories obtained from Case C1 and Case C2 are shown in **Fig.10**. When compared to that obtained from Case C, it can be clearly seen that Case C1 gives higher maximum acceleration with shorter duration of motion. On the contrary, motion with much lower maximum

acceleration and longer shaking duration is obtained from Case C2. The velocity spectra using damping ratio of 5% obtained from Case C, C1 and C2 are shown in **Fig.11**. The velocity amplitude of Case C and C1 (where rupture propagates towards Bangkok) is larger than that of case C2 (where rupture propagates away from Bangkok). Furthermore, predominant period of the motion obtained from Case C1 (=0.65 sec) is lower than those obtained from motions of Case C and C2 (about 1.2 sec.).

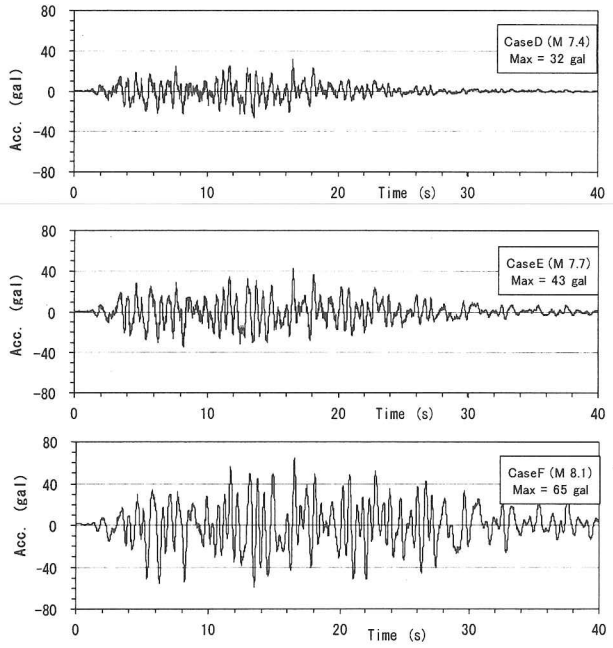

Fig.12 Acceleration time history

4.3 Strong ground motion from Osaki's spectrum

Based on the Osaki's spectrum, the strong ground motion can be estimated. The acceleration time histories obtained for cases with different earthquake magnitudes are shown in **Fig.12**. Their maximum accelerations are summarized in **Table 6**. The magnitudes of earthquakes used in the analysis are 7.4 (Case D), 7.7 (Case E) and 8.1 (Case F), respectively. Osaki's spectrum obviously gives motions with much smaller maximum acceleration when comparing to the empirical Green's function method. On the contrary, the maximum velocity is much larger from the motion obtained from Osaki's spectrum. The velocity spectrums obtained from the analysis using Osaki's spectrum is compared to the targeted spectrums in **Fig.13**. It can be clearly seen that the computed spectrum cannot fit to the targeted spectrum at low period part (high frequency component). Namely motion with period of less than 0.4 sec cannot be represented by the Osaki's spectrum. The maximum spectrum velocities of motions with period longer than 0.5 sec. are 8.5 kine, 13 kine and 23 kine. On the contrary, the amount of short period motion is very small compared to the long period one. This is one the reason why one obtains very different acceleration and velocity time history.

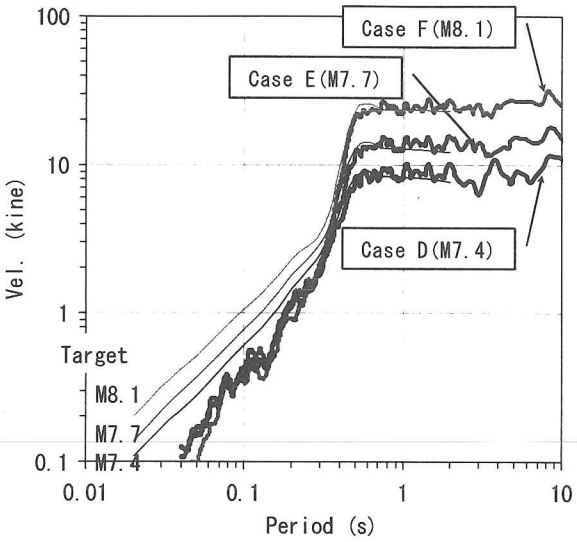

Fig.13 Velocity response spectrum

Table 6 Maximum response

Case	Acc.(gal)	Vel.(kine)
D (M7.4)	31.5	6.05
E (M7.7)	43.2	8.49
F (M8.1)	64.6	15.76

5. Bangkok subsoil characteristics

Fig.14 shows the contour of the ratio of H/V spectrum obtained from micro-tremor test of the Bangkok terrain[11]. The predominant period in the area varies from about 0.4 sec in the north of Bangkok (Ayuthaya) to about 0.8 sec at the coastline of the Gulf of Thailand. Based on this study, Arai and Yamazaki[12] had conducted a series of back-analysis to identify the depth of base rock of the area. They found that the base rock in center of Bangkok could be as deep as 600 – 700 m from the ground surface.

Teachavorasinskun and Lukkunaprasit[13] has conducted the down hole seismic test to explore the shear wave velocity profile of Bangkok subsoil in the center of Bangkok. They found that the shear wave velocity of the top 30 m could be linearly correlated to the depth from the ground surface (Z) as;

$$V_s = 45.4 + 8.8Z \qquad (1)$$

As a consequence, the subsoil profile of Bangkok used in the present study will be those obtained from the center part (as summarized in **Table 7**). The shear wave velocity is estimated from Eqn.(1) for soils at

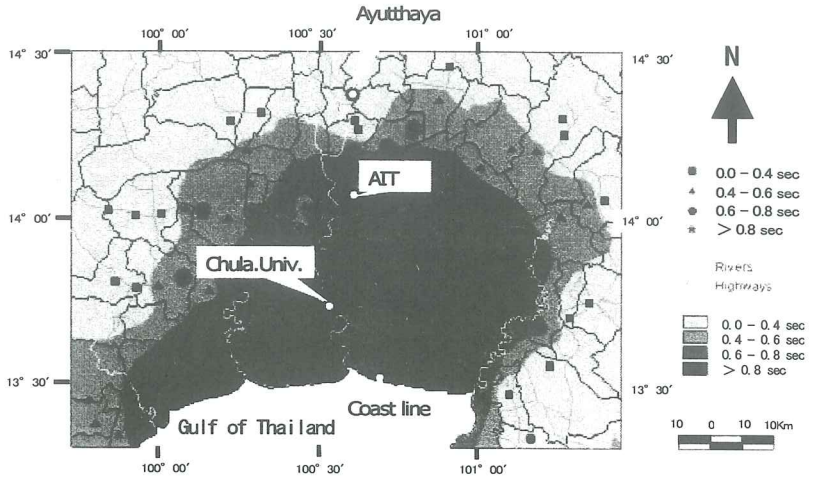

Fig.14 Predominant period of micro-tremor

Table 7 Soil profile at Chula Univ.

Depth (m)	Vs(m/s)	ρ(t/m^3)
0～5	67.4	1.70
5～10	111.4	1.70
10～15	155.4	1.80
15～20	199.4	1.80
20～25	243.4	1.80
25～30	287.4	1.90
30～36	335.8	1.90
36～70	393.0	1.90
70～240	450.0	1.90
240～720	770.0	1.95
720～∞	2000.0	2.00

shallow depth (less than 36 m) and from Yamazaki et al. for soils at greater depth (greater than 36 m).

6. Amplification nature of Bangkok subsoil by using nonlinear response analysis

The acceleration time histories as shown in **Figs.7** and **12** are used as input for the ground response analysis. The input motion will be applied at the soil at depth of 720 m from the ground surface. The ground response analysis was done using the non-linear finite element analysis software FLUSH[14]. The non-linear parameters for soils at depth less than 36 m is shown in **Fig.15**.

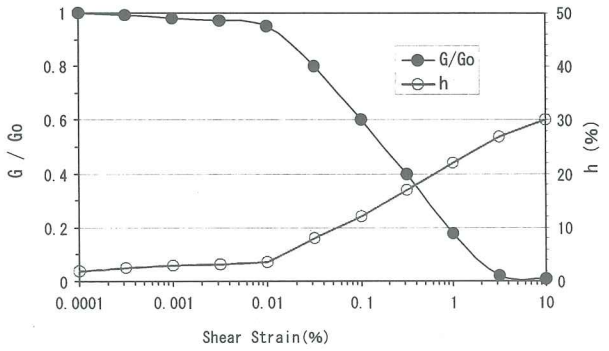

Fig.15 Non-linear soil material

6.1 Responses of Bangkok ground to the strong motions obtained from empirical Green's function method

The response motions of Bangkok subsoil to the strong motion obtained from Case A, Case B and Case C are shown in **Fig.16**. While their maximum acceleration values are summarized in **Table 8**. The amplifications (ratio between the maximum acceleration of the surface to that of the input motion) are also given in **Table 9**. The results obtained from Case D, E and F are also provided in **Tables 8** and **9**. It can be seen that the surface motion contains more wave with longer period

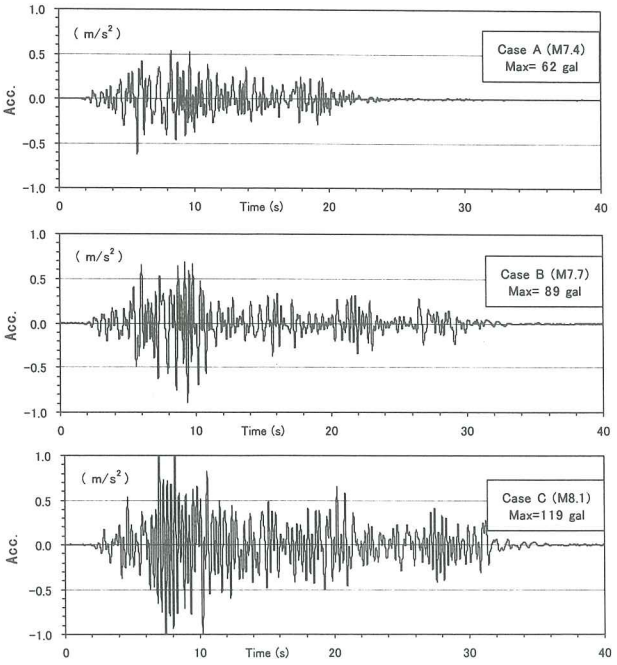

Fig.16 Acceleration time history

Table 8 Maximum response

Case	Acc. (gal)	Vel. (kine)	Case	Acc. (gal)	Vel. (kine)
A	61.9	6.61	D	119.5	21.43
B	89.2	9.04	E	155.8	29.07
C	119.0	13.00	F	243.1	52.27

Table 9 Maximum response amplification

Case	Acc. (gal)	Vel. (kine)	Case	Acc. (gal)	Vel. (kine)
A	1.3	2.2	D	3.8	3.5
B	1.2	1.5	E	3.6	3.4
C	1.1	1.5	F	3.8	3.3

than the input motion with acceleration amplification factor of about 1.1 – 1.3.

The acceleration response spectra (with damping ratio of 5%) of the ground surface motions are summarized in **Fig.17**. The input motion obtained from Case A, B, C, D, E and F are used. It is surprisingly to find the short predominant period of about 0.2 – 0.3 sec can be derived from the acceleration spectrum responses. The maximum accelerations of the surface motion are 250, 450 and 750 gal for cases with input motions from Case A, B and C, respectively.

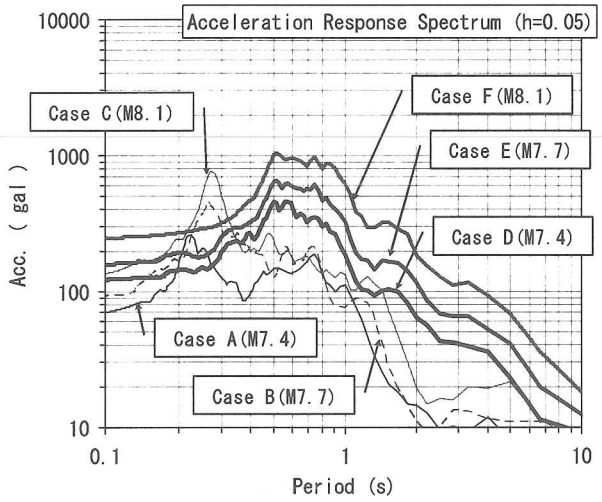

Fig.17 Acceleration response spectrum

6.2 Responses of Bangkok subsoil using strong ground motions from Osaki's spectrum

Fig.18 shows the surface ground motions of Bangkok subsoil when using the strong ground motions from Case D, E and F as input motions. As previously mentioned, the maximum ground surface acceleration and amplification ratio have been given in **Tables 8** and **9**. Compared to results obtained when motions of Case A, B and C are used, the amplification factor obtained from the results using Osaki's spectrum is much higher. The amplification can be as high as 3.0. From the acceleration spectrum, it can be clearly seen that the predominant periods of the surface ground motion varies between 0.5 to 1.0 sec. It should be noted here that the acceleration amplitude at about 0.5 sec is dependent on earthquake magnitudes. Peak spectrum amplitude for Case D, E and F are 450, 600 and 1,000 gal, respectively.

6.3 Transfer function

The transfer functions for Case C and F are plotted in **Fig.19**, together with that obtained from linear elastic analysis. It should be reminded that for Case C and F the

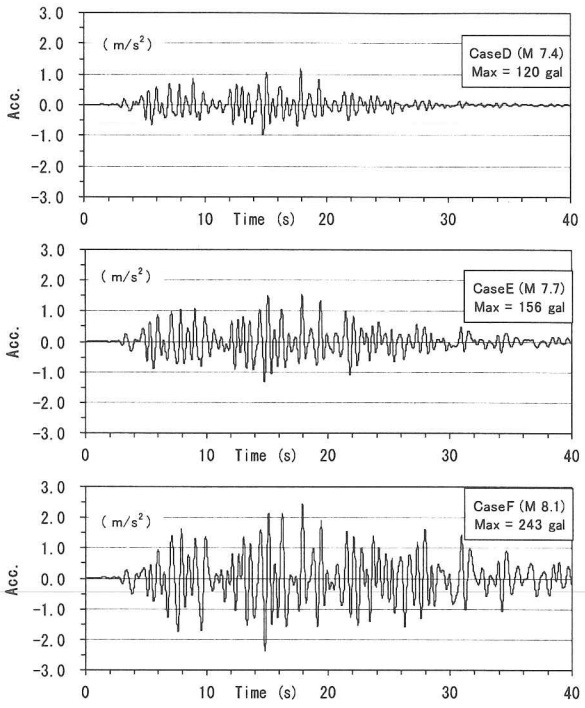

Fig.18 Acceleration time history

stiffness and damping ratio change according to the stiffness (damping) – strain relationship as shown in **Fig.15**. As shown in **Fig.19**, peaks of the transfer function occur at different periods, namely, 0.4 – 0.5 sec for linear analysis, 0.7 – 0.8 sec for Case C and 0.9 sec for Case F. The shift of peak is due to highly non-linear nature of the top 36 m soft soil deposits as mentioned earlier. It can be concluded here that for non-linear material, resonant occurs at around 0.6 – 1.0 sec. Furthermore, the transfer function curves also indicate another two peaks at 1.6 and 3.7 sec. These reflect the nature of deeper subsoil strata.

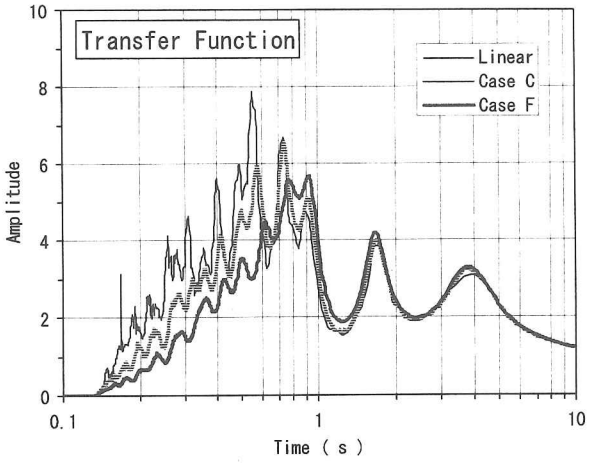

Fig.19 Transfer function

According to the acceleration response spectrum of the surface ground motion, the predominant period when input motions from Case A, B and C are used range between 0.2 – 0.3 sec. This is in well corresponding to the velocity response spectrum of the input motion themselves which peak at 0.27 sec is observed (**Fig.8**). Similarly, predominant period of 0.5 – 1.0 sec can be observed for the surface motion using Case D, E and F as input motions, comparing to the 0.5 sec peak obtained from the spectrum of input motions themselves.

7. Conclusions

The damages caused by earthquakes in Bangkok are still very limited. It has still never experienced the big earthquake of intensity greater than 5(on the Japanese scale). There were quite a few structures which highly susceptible to shaking, for example small housing building with wooden structures, brick and masonry buildings. Furthermore, most of the buildings has not designed to have sufficient resistance to the lateral forces; for example most building lower than 10 floors were built and supported by single pile with very small pile cap (or without pile cap).

The masonry structures, small commercial RC frame building and small wooden structures have resonant period of about 0.1 – 0.3 sec. Medium building (less 10 floors) is usually showing resonant at about 0.7 sec, while the highlight building resonant at 2 – 3 sec. Among these various kinds of structures, the medium building with resonant period of 0.7 sec should be one of the most susceptible to earthquake in Bangkok. This is because (as shown in the curves of the transfer functions in **Fig.19**) the influence of the top soft deposit showing similar predominant period. This means that the medium building and top soft soil might be undergone resonant under earthquake attacks. It has been well recognized that Bangkok always felt the long period motion resulted from the past far-field earthquakes. **Fig. 8** indicates that the strong motion from the Three Pagoda fault may provides motion with have large contents at 1 – 2 sec period. This may greatly affect the 10 – 20 floor buildings.

Acknowledgment

The software for conducting the empirical Green's function and stochastic models has been made available through Prof. Irikura for Kyoto University. The authors would like to express his great appreciation herein.

References

1) SEASEE: Southeast Asia Association of Seismology and Earthquake Engineering Series on Seismology, Volume II, ISBN No.974-8202-13-5, 1995.
2) DMR: Department of Mineral Resource, Thailand, 1999.
3) Bender, F.: Geology of Burma, Gebruder Borntraeger, Berlin, pp.293, 1983.
4) Hartzell, S.H.: Earthquake aftershocks as Green's function, Geophys. Res. Lett., 5, pp.1-4, 1978.
5) Irikura, K.: Prediction of strong acceleration motion using empirical Green's function method, Proc. of 7th Japan Earthquake Eng. Symp., pp.151-156, 1986.
6) Boore, D. M.: Stochastic simulation of high- frequency ground motions based on seismological models of the radiated spectra, Bull. Seism. Soc. Am., Vol.73, No.6, pp.1865-1894, 1983.
7) Osaki, Y.: Introduction on spectrum analysis of earthquake, Kajima publishing co., 2002. (in Japanese)
8) Somerville, P.: Engineering applications of strong ground motion simulation, Tectonophysics, 218, 195-219, 1993
9) Faccioli., E.: A study of strong motions from Italy and Yugoslavia in terms of gross source properties, Geophys. Monograph, 37, Maurice Ewing, AGU, 6, pp.297-309, 1986.
10) Brune, J.N.: Tectonic stress and spectra of seismic shear waves from earthquakes, J. Geophys. Res., 75, pp.4997-5009, 1970.
11) Tulandhar et al : Seismic microzonation of the greater Bangkok using microtremor observation, Proc. of the 8th National Convention on Civil Engineering, Thailand, 1, STR203-206, 2002.
12) Hiroshi Arai and Fumio Yamazaki: Estimation of S-Wave Velocity Profile Using Microtremor Arrays in the Greater Bangkok, Thailand, 38th Annual Convention of JGS, pp.2089-2090, 2003.
13) Teachavorasinskun, S. and Lukkunaprasit, P.: A simple correlation for shear wave velocity of soft Bangkok clays, Geotechnique, 54, No.5, pp.323-326, 2004.
14) Lysmer, H., Udaka, H., Tsai, C. and Bolton, H. : FLUSH-A computer program for approximate 3-D analysis of soil-structure interaction problems, EERC 75-30, 1975.

(Received November 9, 2007)